Emergency Landing for a Quadrotor in Case of a Propeller Failure: A PID Based Approach

Vincenzo Lippiello, Fabio Ruggiero, and Diana Serra

***Abstract*— A controller dealing with the failure of a quadrotor's motor is presented in this paper. Supposing that the failure has been already detected by the system, the quadrotor is modelled as a birotor with fixed propellers and it is controlled to follow a planned emergency landing trajectory. Theory shows that, in such a configuration, the aerial vehicle is allowed to reach any position in the Cartesian space dropping the possibility to control the yaw angle. Simulations are presented to confirm the presented methodology.**

I. Introduction

Service aerial robotics is growing day by day. Vertical Take-off and Landing (VToL) Unmanned Aerial Vehicles (UAVs) are starting to be employed in anthropic environments for several applications. Amazon is planning to deliver packages into customers hands in thirty minutes or less using hexarotors [1]. Moreover, such aerial vehicles are moving from passive tasks like inspection [2] and surveillance [3] into active tasks like grasping [4] and aerial manipulation [5], [6], [7], [8]. This changing scenario requires the introduction not only of rules and regulation, but also of safe controllers.

Therefore, the above depicted scenario requires the design of controllers for safety-critical systems: fault detection, diagnosis and tolerance approaches become thus essential. Fault tolerance methods try to maintain the same functionalities of the system allowing reduced performance when a damage appears [9]. Passive fault tolerant control systems (PFTCS) do not alter the structure of the controller, while the active fault tolerant control systems (AFTCS) reconfigure the control actions to guarantee stability and acceptable performance of the system [10].

In the literature, several methods tackle the problem of controlling a quadrotor in case of sensor [11], [12] and/or motor faults. The latter case is of interest for this paper. A Thau observer is employed in [13] to detect the fault in the aerial vehicle. Assuming that a propeller might lose up to 50% of its efficiency, the model after the failure is estimated in [14] to guarantee the stability of the aerial platform. A sliding mode controller with a Luenberger observer is employed in [15] to distinguish between external disturbances and faults, and reconfigure the controller when a partial failure is present in the quadrotor's propellers. An AFTCS with a Gain Scheduling approach is instead employed in [16] in case of performance loss in each propeller of the quadrotor. A backstepping approach is proposed in [17] to cope with a 25% of reduced performance in the quadrotor's motors. A number of methods have been tested and compared in [18] in case of 50% reduced performance in the propellers. Other methods consider instead the complete failure of a quadrotor's propeller. A feedback linearization with a PD-based controller is employed in [19], but no stability analysis and coupling effects between inner and outer loops are considered. An equidistant trirotor is taken into account in [20], but the designed control law is valid only for spiral motions. A safety landing of a quadrotor with a propeller failure is adopted in [21] through a H-infinity loop shaping method. A LQR controller is exploited in [22] for periodic solutions in case of single, two opposite and three propellers failure. Hexacopters have been recently employed to have redundancy in the system in case of failure of one or more motors.

In this paper, it is assumed that the failure of one of the quadrotor's propellers has been already detected, the controller has been switched to the emergency landing modality and the trajectory has been planned. How such things have been implemented is out of the scope of this paper: one among the techniques illustrated above in the literature review might be employed. The approach here proposed considers to turn off also the propeller aligned on the same quadrotor axis of the broken motor. In this way, the resulting configuration is a *birotor* with fixed propellers[1]. It will be proved that each point in the 3D Cartesian space can be reached by the birotor renouncing to the possibility of controlling the yaw angle: any emergency landing trajectory can be thus tracked. The control is designed by employing a PID based controller, where coupling between inner and outer control loops are explicitly taken into account in the stability proof. In [25] authors have employed a backstepping approach to solve the same issues but theory has covered only regulation cases: this is overcome by using the proposed PID based approach.

II. Modeling

First, the model of a quadrotor is described, then the model of a birotor with fixed propeller is introduced.

Let Σ_i and Σ_b be a world-fixed and a body reference frame, respectively (see Fig. 1). The latter is placed at

Authors are listed in alphabetical order. The research leading to these results has been supported by the SHERPA collaborative project, which has received funding from the European Community 7th Framework Programme (FP7/2007-2013) under grant agreements ICT-600958. The authors are solely responsible for its content.

Vincenzo Lippiello, Fabio Ruggiero and Diana Serra are with the PRISMA Lab, Department of Electrical Engineering and Information Technology, Università degli Studi di Napoli Federico II, via Claudio 21, 80125, Naples, Italy. Corresponding author's email fabio.ruggiero@unina.it

[1]In the literature, a birotor is typically referred to as an aerial vehicle with two propellers whose alignment can be tilted through other two actuators [23], [24]

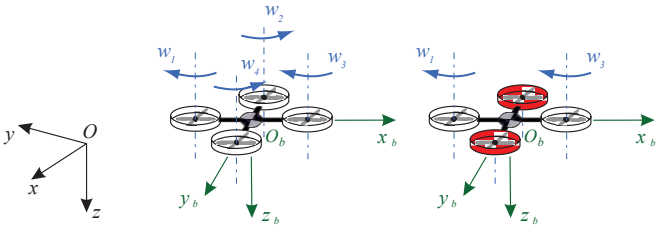

Fig. 1. Left. The quadrotor and related frames: black, the inertial frame Σ_i; green, the body frame Σ_b; blue, the speed and label of each motor. Right. The birotor configuration with in red the turned off propellers.

the center of mass of the quadrotor. The rotation matrix $\boldsymbol{R}_b(\boldsymbol{\eta}_b) \in SO(3)$ defines the attitude of Σ_b with respect to Σ_i, where $\boldsymbol{\eta}_b = \begin{bmatrix}\phi & \theta & \psi\end{bmatrix}^{\mathrm{T}} \in \mathbb{R}^3$ is the roll-pitch-yaw Euler angles vector representing the attitude of the quadrotor. Let $\dot{\boldsymbol{\eta}}_b = \begin{bmatrix}\dot{\phi} & \dot{\theta} & \dot{\psi}\end{bmatrix}^{\mathrm{T}} \in \mathbb{R}^3$ and $\ddot{\boldsymbol{\eta}}_b = \begin{bmatrix}\ddot{\phi} & \ddot{\theta} & \ddot{\psi}\end{bmatrix}^{\mathrm{T}} \in \mathbb{R}^3$ be the first and second time derivatives of $\boldsymbol{\eta}_b$, respectively, and $\boldsymbol{\omega}_b^b \in \mathbb{R}^3$ be the angular velocity of the aerial vehicle in the body frame Σ_b. The linear relationship $\boldsymbol{\omega}_b^b = \boldsymbol{Q}(\boldsymbol{\eta}_b)\dot{\boldsymbol{\eta}}_b$ holds in both directions within the following assumption.

- **Assumption 1.** The aerial vehicle does not pass through representation singularities: the allowable configuration space for the roll-pitch-yaw angles $\boldsymbol{\eta}_b$ is $\mathcal{Q} = \{\boldsymbol{\eta}_b \in \mathbb{R}^3 : \theta \neq \pi/2 + k\pi, \phi \neq \pi/2 + k\pi, k \in \mathbb{Z}\}$.

The detailed expressions for $\boldsymbol{R}_b(\boldsymbol{\eta}_b)$ and $\boldsymbol{Q}(\boldsymbol{\eta}_b)$ can be found in [25], [26].

The dynamic equations of the quadrotor are retrieved employing the Newton-Euler formulation [27]

$$m\ddot{\boldsymbol{p}}_b = m\boldsymbol{g} + \boldsymbol{R}_b(\boldsymbol{\eta}_b)\boldsymbol{f}_b^b, \tag{1a}$$
$$\boldsymbol{I}_b\dot{\boldsymbol{\omega}}_b^b = -\boldsymbol{S}(\boldsymbol{\omega}_b^b)\boldsymbol{I}_b\boldsymbol{\omega}_b^b - \boldsymbol{g}_a - \boldsymbol{F}_o\boldsymbol{\omega}_b^b + \boldsymbol{\tau}_b^b, \tag{1b}$$
$$\dot{\boldsymbol{R}}_b(\boldsymbol{\eta}_b) = \boldsymbol{R}_b(\boldsymbol{\eta}_b)\boldsymbol{S}(\boldsymbol{\omega}_b^b), \tag{1c}$$

where $\boldsymbol{p}_b = \begin{bmatrix}x & y & z\end{bmatrix}^{\mathrm{T}}$ is the position of the aerial vehicle expressed in Σ_i, and $\dot{\boldsymbol{p}}_b = \begin{bmatrix}\dot{x} & \dot{y} & \dot{z}\end{bmatrix}^{\mathrm{T}}$ and $\ddot{\boldsymbol{p}}_b = \begin{bmatrix}\ddot{x} & \ddot{y} & \ddot{z}\end{bmatrix}^{\mathrm{T}} \in \mathbb{R}^3$ are the related time derivatives; m denotes the mass of the aerial vehicle; $\boldsymbol{g} = \begin{bmatrix}0 & 0 & g\end{bmatrix}^{\mathrm{T}} \in \mathbb{R}^3$ is the gravity vector, with $g = 9.81$ m/s^2; $\boldsymbol{I}_b = \mathrm{diag}(\begin{bmatrix}I_x & I_y & I_z\end{bmatrix}) \in \mathbb{R}^{3\times3}$ is the constant inertia matrix of the quadrotor expressed in Σ_b; $\boldsymbol{g}_a = I_p\boldsymbol{S}(\boldsymbol{\omega}_b^b)\boldsymbol{e}_3(\omega_1 + \omega_2 + \omega_3 + \omega_4)$ is the gyroscopic torques due to the combination of the aerial vehicle rotation and the propellers, with ω_i the speed of the ith propeller, $i = 1, \ldots, 4$, and I_p its inertia; $\boldsymbol{e}_3 = \begin{bmatrix}0 & 0 & 1\end{bmatrix}^{\mathrm{T}}$ and $\boldsymbol{S}(\cdot) \in \mathbb{R}^{3\times3}$ denotes the skew-symmetric operator; $\boldsymbol{F}_o \in \mathbb{R}^{3\times3}$ is a diagonal positive definite matrix denoting the air friction coefficient[2]; $\boldsymbol{f}_b^b \in \mathbb{R}^3$ and $\boldsymbol{\tau}_b^b \in \mathbb{R}^3$ are the forces and torques input vectors, respectively, expressed in Σ_b.

In the considered case of a quadrotor, the expressions of the input force and torque are related to four main control inputs, namely: three control torques around each axis of the body frame Σ_b and the total thrust $u > 0$ perpendicular to the propellers rotation plane. In detail $\boldsymbol{\tau}_b^b = \begin{bmatrix}\tau_\phi & \tau_\theta & \tau_\psi\end{bmatrix}^{\mathrm{T}}$, and $\boldsymbol{f}_b^b = \begin{bmatrix}0 & 0 & u\end{bmatrix}^{\mathrm{T}}$. Neglecting both the air friction terms and $\boldsymbol{g}_a$ in (1) and writing the dynamic equations with respect to Σ_i, a simplified model can be considered to design the control law

$$m\ddot{\boldsymbol{p}}_b - m\boldsymbol{g} = -u\boldsymbol{R}_b(\boldsymbol{\eta}_b)\boldsymbol{e}_3, \tag{2a}$$
$$\boldsymbol{M}(\boldsymbol{\eta}_b)\ddot{\boldsymbol{\eta}}_b + \boldsymbol{C}(\boldsymbol{\eta}_b, \dot{\boldsymbol{\eta}}_b)\dot{\boldsymbol{\eta}}_b = \boldsymbol{Q}(\boldsymbol{\eta}_b)^{\mathrm{T}}\boldsymbol{\tau}_b^b, \tag{2b}$$

with $\boldsymbol{M}(\boldsymbol{\eta}_b) = \boldsymbol{Q}(\boldsymbol{\eta}_b)^{\mathrm{T}}\boldsymbol{I}_b\boldsymbol{Q}(\boldsymbol{\eta}_b) \in \mathbb{R}^{3\times3}$, $\boldsymbol{\eta}_b \in \mathcal{Q}$, the symmetric and positive definite inertia matrix, and $\boldsymbol{C}(\boldsymbol{\eta}_b, \dot{\boldsymbol{\eta}}_b) = \boldsymbol{Q}^{\mathrm{T}}\boldsymbol{S}(\boldsymbol{Q}\dot{\boldsymbol{\eta}}_b)\boldsymbol{I}_b\boldsymbol{Q} + \boldsymbol{Q}^{\mathrm{T}}\boldsymbol{I}_b\dot{\boldsymbol{Q}} \in \mathbb{R}^{3\times3}$ the Coriolis matrix, where $\dot{\boldsymbol{Q}} \in \mathbb{R}^{3\times3}$ is the time derivative of $\boldsymbol{Q}(\boldsymbol{\eta}_b)$.

The relationships between the thrust, the control torques for each quadrotor's axis and the squared motor speeds w_i^2, with $i = 1, \ldots, 4$, are given by [28]

$$u = \rho_u(w_1^2 + w_2^2 + w_3^2 + w_4^2), \tag{3a}$$
$$\tau_\phi = l\rho_u(w_2^2 - w_4^2), \tag{3b}$$
$$\tau_\theta = l\rho_u(w_3^2 - w_1^2), \tag{3c}$$
$$\tau_\psi = cw_1^2 - cw_2^2 + cw_3^2 - cw_4^2, \tag{3d}$$

where l is the distance between each motor and the center of mass of the quadrotor, $\rho_u > 0$ and $c > 0$ are the thrust and drag factors, respectively.

Suppose without loss of generality that motor 2 is broken, i.e., $w_2 = 0$ in (3). From (3b) it is possible to notice that a generic τ_ϕ can not be arbitrarily assigned: motor 4 creates a torque around the x-axis of Σ_b only in one direction (assuming that the rotational direction of each propeller is fixed, as in the most currently available off-the-shelf devices). Therefore, it is not possible to control the rotation around the axis of Σ_b which is perpendicular to the axis where the broken motor is placed. The assumption to turn off also the motor placed on the same axis of the broken one is thus made in this paper[3], i.e., $w_4 = 0$ if motor 2 is broken (see Fig. 1, right). The resulting configuration is hence a birotor with fixed propellers. The related dynamic model is equivalent to (2) but the relationships between the thrust, the control torques and the squared motor speeds differ as follows

$$u = \rho_u(w_1^2 + w_3^2), \tag{4a}$$
$$\tau_\phi = 0, \tag{4b}$$
$$\tau_\theta = l\rho_u(w_3^2 - w_1^2), \tag{4c}$$
$$\tau_\psi = cw_1^2 + cw_3^2. \tag{4d}$$

Similar equations can be obtained by considering a failure on motor 1 and/or 3. The case of two broken motors not aligned on the same quadrotor's axis is out of the scope of this paper.

III. Control Law

Notice that τ_ψ in (4d) can not be controlled arbitrarily since it is not possible to change its sign. Hence, it is possible to independently control only the thrust and the

[2]In general, the expression of the air drag might be more complicated depending, for instance, from the square of the velocity.

[3]The case in which all the three remaining propellers are active is considered in [22].

torque around the y-axis of the quadrotor. Substituting (4a) in (4d) yields

$$\tau_\psi = \overline{\tau}_\psi = cu/\rho_u, \tag{5}$$

representing the spinning torque of the aerial vehicle around its z-axis and depending on the current thrust and the aerodynamic parameters ρ_u and c. Therefore, the birotor has the peculiarity to continuously spin around its vertical axis making not possible to control the yaw angle. It is still possible to control the thrust and the pitch angle independently.

Recalling Assumption 1, the following control law

$$\tau_\theta = \left(I_y c_\phi + I_y s_\phi^2/c_\phi\right)\overline{\tau}_\theta + \alpha_1(\boldsymbol{\eta}, \dot{\boldsymbol{\eta}}, \overline{\tau}_\psi), \tag{6}$$

can be considered with $\overline{\tau}_\theta$ a virtual control input and

$$\begin{aligned}
\alpha_1 &= I_y s_\phi(\overline{\tau}_\psi - \alpha_2(\boldsymbol{\eta}, \dot{\boldsymbol{\eta}}))/(I_z c_\phi) + \alpha_3(\boldsymbol{\eta}, \dot{\boldsymbol{\eta}}),\\
\alpha_2 &= -I_x\dot{\phi}\dot{\theta}c_\phi + I_y\dot{\phi}\dot{\theta}c_\phi - I_z\dot{\phi}\dot{\theta}c_\phi + I_x\dot{\psi}^2 c_\theta s_\phi s_\theta\\
&\quad - I_y\dot{\psi}^2 c_\theta s_\phi s_\theta - I_x\dot{\phi}\dot{\psi}c_\theta s_\phi + I_y\dot{\phi}\dot{\psi}c_\theta s_\phi\\
&\quad - I_z\dot{\phi}\dot{\psi}c_\theta s_\phi + I_x\dot{\psi}\dot{\theta}c_\phi s_\theta - I_y\dot{\psi}\dot{\theta}c_\phi s_\theta - I_z\dot{\psi}\dot{\theta}c_\phi s_\theta,\\
\alpha_3 &= -I_x\dot{\phi}\dot{\theta}s_\phi - I_y\dot{\phi}\dot{\theta}s_\phi + I_z\dot{\phi}\dot{\theta}s_\phi - I_x\dot{\psi}^2 c_\phi c_\theta s_\theta\\
&\quad + I_z\dot{\psi}^2 c_\phi c_\theta s_\theta + I_x\dot{\phi}\dot{\psi}c_\phi c_\theta + I_y\dot{\phi}\dot{\psi}c_\phi c_\theta\\
&\quad - I_z\dot{\phi}\dot{\psi}c_\phi c_\theta + I_x\dot{\psi}\dot{\theta}s_\phi s_\theta - I_y\dot{\psi}\dot{\theta}s_\phi s_\theta - I_z\dot{\psi}\dot{\theta}s_\phi s_\theta.
\end{aligned}$$

Substituting (6) in (2b) and considering (4b) and (5) yield

$$\ddot{\theta} = \overline{\tau}_\theta, \tag{7}$$

meaning that it is possible to control the pitch angle through a proper choice of the virtual control input $\overline{\tau}_\theta$. Denoting with $\ddot{\theta}_d$, $\dot{\theta}_d$ and θ_d the desired acceleration, velocity and value of the pitch angle, respectively, the following simple PD controller is chosen

$$\overline{\tau}_\theta = \ddot{\theta}_d + k_{d,\theta}\dot{e}_\theta + k_{p,\theta}e_\theta, \tag{8}$$

with $e_\theta = \theta_d - \theta$, $\dot{e}_\theta = \dot{\theta}_d - \dot{\theta}$, $\ddot{e}_\theta = \ddot{\theta}_d - \ddot{\theta}$, and $k_{p,\theta}$ and $k_{d,\theta}$ two positive gains.

A new virtual input acceleration $\boldsymbol{\mu} = \begin{bmatrix}\mu_x & \mu_y & \mu_z\end{bmatrix}^{\mathrm{T}} \in \mathbb{R}^3$ can be introduced and it is defined by

$$\boldsymbol{\mu} = -(u/m)\boldsymbol{R}_b(\phi, \theta_d, \psi)\boldsymbol{e}_3 + \boldsymbol{g}, \tag{9}$$

representing the desired acceleration vector expressed in Σ_i, in which the magnitude is the thrust u produced by the remaining propellers, while the orientation is given by the desired pitch and the current measured roll and yaw. Replacing $\theta = \theta_d - e_\theta$ in (2a), taking into account (9) and the following trigonometric relationships

$$\begin{aligned}
\sin(a-b) &= \sin(a) - 2\sin(b/2)\cos(a - b/2)\\
\cos(a-b) &= \cos(a) + 2\sin(b/2)\sin(a - b/2)
\end{aligned}$$

yields

$$\ddot{\boldsymbol{p}}_b = \boldsymbol{\mu} + (u/m)\boldsymbol{\delta}(\boldsymbol{\eta}_b, \theta_d, e_\theta), \tag{10}$$

where $\boldsymbol{\delta}(\boldsymbol{\eta}_b, \theta_d, e_\theta) = \begin{bmatrix}\delta_x & \delta_y & \delta_z\end{bmatrix}^{\mathrm{T}} \in \mathbb{R}^3$ is the following interconnection vector

$$\delta_x = 2\cos(\phi)\cos(\psi)\sin(e_\theta/2)\cos(\theta_d - e_\theta/2), \tag{11a}$$

$$\delta_y = 2\cos(\phi)\sin(\psi)\sin(e_\theta/2)\cos(\theta_d - e_\theta/2), \tag{11b}$$

$$\delta_z = -2\cos(\phi)\sin(e_\theta/2)\sin(\theta_d - e_\theta/2). \tag{11c}$$

The virtual control input $\boldsymbol{\mu}$ can be thus chosen as follows

$$\boldsymbol{\mu} = \ddot{\boldsymbol{p}}_d + \boldsymbol{K}_p\boldsymbol{e}_p + \boldsymbol{K}_d\dot{\boldsymbol{e}}_p, \tag{12}$$

where $\boldsymbol{K}_p$, $\boldsymbol{K}_d \in \mathbb{R}^{3\times 3}$ are positive definite gain matrices, $\boldsymbol{p}_d$, $\dot{\boldsymbol{p}}_d$, $\ddot{\boldsymbol{p}}_d \in \mathbb{R}^3$ represent the desired position trajectory for the birotor, and $\boldsymbol{e}_p = \boldsymbol{p}_d - \boldsymbol{p}_b$, $\dot{\boldsymbol{e}}_p = \dot{\boldsymbol{p}}_d - \dot{\boldsymbol{p}}_b$, $\ddot{\boldsymbol{e}}_p = \ddot{\boldsymbol{p}}_d - \ddot{\boldsymbol{p}}_b \in \mathbb{R}^3$ are the related tracking errors.

Folding (12) in (10) and (8) in (7) yields the following closed-loop equations

$$\ddot{\boldsymbol{e}}_p + \boldsymbol{K}_d\dot{\boldsymbol{e}}_p + \boldsymbol{K}_p\boldsymbol{e}_p = -(u/m)\boldsymbol{\delta}(\boldsymbol{\eta}_b, \theta_d, e_\theta), \tag{13a}$$

$$\ddot{e}_\theta + k_{d,\theta}\dot{e}_\theta + k_{p,\theta}e_\theta = 0. \tag{13b}$$

- **Remark 1.** The closed-loop equations in (13) are equivalent to generalized mechanical impedances with programmable stiffness and damping through a proper choice of the gains. An external disturbance is present in (13a) due to the coupling between angular and linear parts through e_θ, θ_d and $\boldsymbol{\eta}_b$.
- **Remark 2.** Two PD controllers have been employed in (8) and (12). As noticed in [28], an integral action can be added to increase tracking accuracy without destroying the stability properties provided in the next section.

To recap, the proposed architecture is depicted in the block-scheme of Fig. 2. After computed the position tracking errors $\boldsymbol{e}_p$ and $\dot{\boldsymbol{e}}_p$, knowing the feedforward acceleration $\ddot{\boldsymbol{p}}_d$, the virtual control input $\boldsymbol{\mu}$ can be computed as in (12). The desired thrust u and the pitch angle θ_d can be computed by inverting (9) as follows

$$u = m\sqrt{\mu_x^2 + \mu_y^2 + (\mu_z - g)^2}, \tag{14a}$$

$$\theta_d = \tan^{-1}((\mu_x c_\psi + \mu_y s_\psi)/(\mu_z - g)), \tag{14b}$$

where ψ is retrieved by the IMU measurements. A second-order low-pass digital filter might be employed to reduce noise and compute both first and second derivatives of θ_d, and hence compute in turn the pitch tracking errors e_θ and $\dot{e}_\theta$. The control input τ_θ is then computed as in (6), with $\overline{\tau}_\theta$ obtained as in (8). Having both the thrust and τ_θ, the propeller inputs for the birotor can be computed inverting (4a) and (4c).

- **Remark 3.** Similar considerations can be made in case of motor 1 and/or 3 failure. In such event, the desired angle is the roll whose desired value can be computed by inverting $\boldsymbol{\mu} = -(u/m)\boldsymbol{R}_b(\phi_d, \theta, \psi)\boldsymbol{e}_3 + \boldsymbol{g}$ and obtaining $\phi_d = \sin^{-1}\left(m(\mu_y c_\psi - \mu_x s_\psi)/u\right)$.

IV. Stability proof

In this section it is shown that the tracking errors in (13) go uniformly asymptotically to zero. However, the state of the birotor includes also the roll and yaw angles and their time derivatives: notice that these quantities are not directly controlled. The behaviour of the uncontrolled accelerations is studied neglecting Coriolis terms for simplicity. Anyway, in the simulations of Section V, the related time histories are depicted and more deep critical comments are provided.

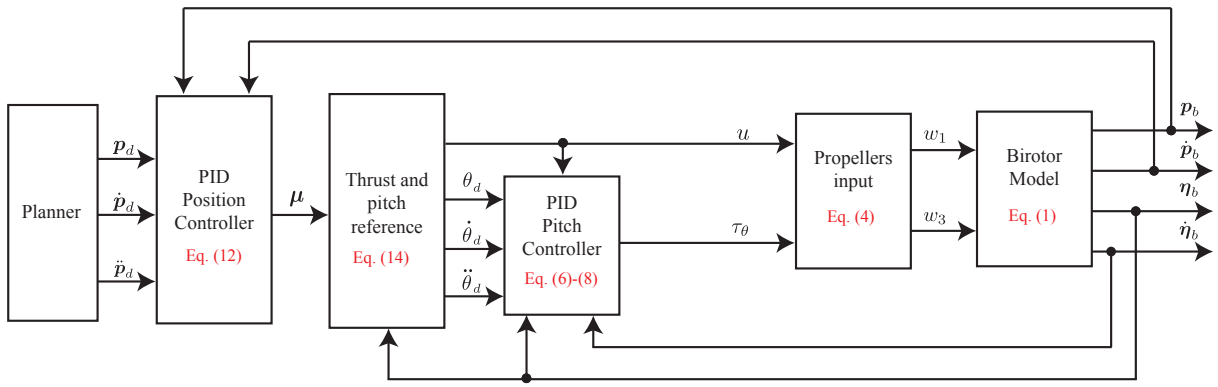

Fig. 2. Block scheme of the proposed control architecture. In red, the corresponding equations in the paper related to each block.

Let $\boldsymbol{x}_1 = \begin{bmatrix}\boldsymbol{e}_p^{\mathrm{T}} & \dot{\boldsymbol{e}}_p^{\mathrm{T}}\end{bmatrix}^{\mathrm{T}} \in \mathbb{R}^6$ and $\boldsymbol{x}_2 = \begin{bmatrix}e_\theta & \dot{e}_\theta\end{bmatrix}^{\mathrm{T}} \in \mathbb{R}^2$ be two vectors denoting the state of the closed-loop system equations (13a) and (13b), respectively, that can also be arranged in the following way

$$\dot{\boldsymbol{x}}_1 = \boldsymbol{\alpha}_1(\boldsymbol{x}_1, \boldsymbol{K}_p, \boldsymbol{K}_d) + \boldsymbol{\beta}_1(u, m, \boldsymbol{\eta}_b, \theta_d, e_\theta), \tag{15a}$$
$$\dot{\boldsymbol{x}}_2 = \boldsymbol{\alpha}_2(\boldsymbol{x}_2, k_{p,\theta}, k_{d,\theta}), \tag{15b}$$

where

$$\boldsymbol{\alpha}_1(\boldsymbol{x}_1, \boldsymbol{K}_p, \boldsymbol{K}_d) = \begin{bmatrix}\dot{\boldsymbol{e}}_p \\ -\boldsymbol{K}_d\dot{\boldsymbol{e}}_p - \boldsymbol{K}_p\boldsymbol{e}_p\end{bmatrix},$$
$$\boldsymbol{\alpha}_2(\boldsymbol{x}_2, k_{p,\theta}, k_{d,\theta}) = \begin{bmatrix}\dot{e}_\theta \\ -k_{d,\theta}\dot{e}_\theta - k_{p,\theta}e_\theta\end{bmatrix},$$
$$\boldsymbol{\beta}_1(u, m, \boldsymbol{\eta}_b, \theta_d, e_\theta) = \begin{bmatrix}\boldsymbol{0}_3 \\ -(u/m)\boldsymbol{\delta}(\boldsymbol{\eta}_b, \theta_d, e_\theta)\end{bmatrix},$$

in which $\boldsymbol{0}_n \in \mathbb{R}^n$ is a n-dimensional null vector. Define the *nominal* system as the closed-loop equation (15a) without the perturbation term $\boldsymbol{\beta}_1(u, m, \boldsymbol{\eta}_b, \theta_d, e_\theta)$

$$\dot{\boldsymbol{x}}_1 = \boldsymbol{\alpha}_1(\boldsymbol{x}_1, \boldsymbol{K}_p, \boldsymbol{K}_d). \tag{16}$$

Consider the next reasonable assumption.

- **Assumption 2.** The planned linear acceleration is bounded as follows

$$\|\ddot{\boldsymbol{p}}_d\| \leq \|\ddot{\boldsymbol{p}}_d\|_{\max} = B, \tag{17}$$

with $B > 0$. In this paper all the norms are Euclidean.

The following theorem [29] is exploited to prove the global uniformly asymptotically stability of (15).

Theorem 1. *Consider the perturbed systems* (15)*, and the related nominal systems* (16) *and* (15b) *for which* $\boldsymbol{x}_1 = \boldsymbol{0}_6$ *and* $\boldsymbol{x}_2 = \boldsymbol{0}_2$ *are two equilibrium points, respectively. Suppose* $V_1(t, \boldsymbol{x}_1)$ *and* $V_2(t, \boldsymbol{x}_2)$ *are two Lyapunov functions of* (16) *and* (15b)*, respectively, satisfying the following inequalities*

$$\partial V_i/\partial t + (\partial V_i/\partial \boldsymbol{x}_i)\boldsymbol{\alpha}_i \leq -\gamma_i\Phi_i^2(\boldsymbol{x}_i), \tag{18a}$$
$$\|\partial V_i/\partial \boldsymbol{x}_i\| \leq \nu_i\Phi_i(\boldsymbol{x}_i), \tag{18b}$$

for all $t > 0$*, where* $\gamma_i > 0$*,* $\nu_i > 0$ *and* $\Phi_i(\boldsymbol{x}_i)$ *is a positive definite and continuous function, with* $i = 1, 2$*. Moreover, the perturbation term in* (15a) *has to satisfy the following inequality*

$$\|\boldsymbol{\beta}_1(u, m, \boldsymbol{\eta}_b, \theta_d, e_\theta)\| \leq \xi_1\Phi_1(\boldsymbol{x}_1) + \xi_2\Phi_2(\boldsymbol{x}_2) \tag{19}$$

with $\xi_i \geq 0$*. Suppose the matrix* $\boldsymbol{S} \in \mathbb{R}^{2\times 2}$ *given by*

$$\boldsymbol{S} = \begin{bmatrix}\gamma_1 - \nu_1\xi_1 & -\nu_1\xi_2 \\ 0 & \gamma_2\end{bmatrix} \tag{20}$$

is a M-matrix[4]*. Then,* $\boldsymbol{x}_1 = \boldsymbol{0}_6$ *and* $\boldsymbol{x}_2 = \boldsymbol{0}_2$ *are globally uniformly asymptotically stable equilibrium points of the system* (15)*.*

Proof. The nominal system (16) has an unique equilibrium point $\boldsymbol{x}_1 = \boldsymbol{0}_6$ since it is a linear system with an associated Hurwitz state matrix $\boldsymbol{A}_1 \in \mathbb{R}^{6\times 6}$ given by

$$\boldsymbol{A}_1 = \begin{bmatrix}\boldsymbol{O}_3 & \boldsymbol{I}_3 \\ -\boldsymbol{K}_p & -\boldsymbol{K}_d\end{bmatrix},$$

where $\boldsymbol{O}_n$, $\boldsymbol{I}_n \in \mathbb{R}^{n\times n}$ are zero and identity matrices of proper dimensions, respectively. Therefore, the following function $V_1(\boldsymbol{x}_1) = (1/2)\boldsymbol{x}_1^{\mathrm{T}}\boldsymbol{P}_1\boldsymbol{x}_1$, is a Lyapunov function for (16), in which $\boldsymbol{P}_1 \in \mathbb{R}^{6\times 6}$ is a positive definite symmetric matrix solving $\boldsymbol{A}_1\boldsymbol{P}_1 + \boldsymbol{P}_1\boldsymbol{A}_1^{\mathrm{T}} + \boldsymbol{\Lambda}_1 = \boldsymbol{O}_6$, for any positive definite symmetric matrix $\boldsymbol{\Lambda}_1 \in \mathbb{R}^{6\times 6}$. Inequalities (18) are then satisfied with [29]

$$\gamma_1 = \underline{\lambda}_{\Lambda_1},\ \nu_1 = 2\overline{\lambda}_{P_1},\ \Phi_1(\boldsymbol{x}_1) = \|\boldsymbol{x}_1\|,$$

where $\underline{\lambda}_\times$ and $\overline{\lambda}_\times$ denote the minimum and maximum eigenvalues, respectively, of a squared matrix. In the same way, the nominal system (15b) has an associated Hurwitx state matrix $\boldsymbol{A}_2 \in \mathbb{R}^{2\times 2}$

$$\boldsymbol{A}_2 = \begin{bmatrix}0 & 1 \\ -k_{p,\theta} & -k_{d,\theta}\end{bmatrix}.$$

The following function $V_2(\boldsymbol{x}_2) = (1/2)\boldsymbol{x}_2^{\mathrm{T}}\boldsymbol{P}_2\boldsymbol{x}_2$, is a Lyapuonov function for (15b), in which $\boldsymbol{P}_2 \in \mathbb{R}^{2\times 2}$ is a positive definite symmetric matrix solving $\boldsymbol{A}_2\boldsymbol{P}_2 + \boldsymbol{P}_2\boldsymbol{A}_2^{\mathrm{T}} + \boldsymbol{\Lambda}_2 = \boldsymbol{O}_2$, for any postive definite symmetric matrix $\boldsymbol{\Lambda}_2 \in \mathbb{R}^{2\times 2}$. Inequalities (18) are then satisfied with

$$\gamma_2 = \underline{\lambda}_{\Lambda_2},\ \nu_2 = 2\overline{\lambda}_{P_2},\ \Phi_2(\boldsymbol{x}_2) = \|\boldsymbol{x}_2\|.$$

[4]A matrix is called a M-matrix if each off-diagonal element is less or at least equal to zero and if each principal minor is positive [29].

In order to verify (19), the bounds for both the thrust u and the perturbation term $\boldsymbol{\delta}(\boldsymbol{\eta}_b, \theta_d, e_\theta)$ are provided. Taking into account (9), (12), (17), the following bound holds

$$\begin{aligned} |u| &= m\|\ddot{\boldsymbol{p}}_d + \boldsymbol{g} - \boldsymbol{K}_p \boldsymbol{e}_p - \boldsymbol{K}_d \dot{\boldsymbol{e}}_p\| \\ &\leq m(B+g) + m\sqrt{2}\max\{\overline{\lambda}_{K_p}, \overline{\lambda}_{K_d}\}\|\boldsymbol{x}_1\|. \end{aligned} \tag{21}$$

Considering the components of the term $\boldsymbol{\delta}(\boldsymbol{\eta}_b, \theta_d, e_\theta)$ in (11), the following bounds can be verified

$$|\delta_x| \leq |e_\theta|,\ |\delta_y| \leq |e_\theta|,\ |\delta_z| \leq |e_\theta|, \tag{22}$$

where $|\cdot|$ denotes the absolute value and in which the following relationships

$$|\sin(e_\theta/2)| \leq |e_\theta/2|,\ |\sin(a)| \leq 1,\ |\cos(a)| \leq 1, \tag{23}$$

with $a = \{\theta_d - e_\theta/2, \psi, \phi\}$, have been employed. Taking into account (22) yields

$$\|\boldsymbol{\delta}(\boldsymbol{\eta}_b, \theta_d, e_\theta)\| = \sqrt{\delta_x^2 + \delta_y^2 + \delta_z^2} \leq \sqrt{3}|e_\theta|. \tag{24}$$

Since the following inequalities holds

$$|e_\theta| \leq \|\boldsymbol{x}_2\|,$$

and taking into account (21) and (24), the following bound of the perturbation term $\boldsymbol{\beta}_1(u, m, \boldsymbol{\eta}_b, \theta_d, e_\theta)$ can be provided

$$\begin{aligned} \|\boldsymbol{\beta}_1\| &\leq \sqrt{3}(B + g + \sqrt{2}\max\{\overline{\lambda}_{K_p}, \overline{\lambda}_{K_d}\}\|\boldsymbol{x}_1\|)\|\boldsymbol{x}_2\| \\ &\leq \sqrt{3}(B + g + \chi\sqrt{2}\max\{\overline{\lambda}_{K_p}, \overline{\lambda}_{K_d}\})\|\boldsymbol{x}_2\|, \end{aligned} \tag{25}$$

where it has been supposed that $\|\boldsymbol{x}_1\| \leq \chi$, with $\chi > 0$ an arbitrary constant. Hence, taking into account (25), inequality (19) is verified with

$$\xi_1 = 0,\ \xi_2 = \sqrt{3}(B + g + \chi\sqrt{2}\max\{\overline{\lambda}_{K_p}, \overline{\lambda}_{K_d}\}).$$

Matrix $\boldsymbol{S}$ in (20) is then equal to

$$\boldsymbol{S} = \begin{bmatrix} \underline{\lambda}_{\Lambda_1} & -2\overline{\lambda}_{P_1}\sqrt{3}(B + g + \chi\sqrt{2}\max\{\overline{\lambda}_{K_p}, \overline{\lambda}_{K_d}\}) \\ 0 & \underline{\lambda}_{\Lambda_2} \end{bmatrix},$$

which could be easily verified is a M-matrix for any value of χ, that could be thus taken as $\chi = \infty$ without putting any restriction to $\boldsymbol{x}_1$ and then keeping global the whole derivation.

Since the assumptions of the Theorem 1 has been verified, the proof continues as in [29], and then $\boldsymbol{x}_1 = \boldsymbol{0}_6$ and $\boldsymbol{x}_2 = \boldsymbol{0}_2$ are globally uniformly asymptotically stable equilibrium points of (15). □

The other state variables of the birotor are now analysed. Neglecting the Coriolis terms in (2b) and taking into account (4b) and (5) yield

$$\begin{aligned} \ddot{\phi} &= -\frac{\sin(e_\theta - \theta_d)(I_z \tau_\theta s_\phi + I_y \overline{\tau}_\psi c_\phi)}{I_y I_z \cos(e_\theta - \theta_d)}, \\ \ddot{\psi} &= \left(I_z \tau_\theta s_\phi + I_y \overline{\tau}_\psi c_\phi\right) / \left(I_y I_z \cos(e_\theta - \theta_d)\right), \end{aligned}$$

whose absolute values can be both bounded by

$$\ddot{\phi}_{max} = \ddot{\psi}_{max} = (\rho_u I_z |\tau_\theta| + c I_y |u|)/(\rho_u I_y I_z |\cos(e_\theta - \theta_d)|),$$

where (5) and (23) have been considered. Then, it can be noticed how the maximum roll and yaw accelerations depend on the inertia and aerodynamic parameters, the thrust, the applied pitch torque, the desired pitch and the related error. Notice that the denominator is not a problem thanks to Assumption 1. Moreover, since Theorem 1 holds, the thrust is limited and the actuated torque is bounded as well, even because there are saturations in the actuators, then the accelerations are bounded. For a deep analysis, even the Coriolis terms should be included, but the expressions become cumbersome. Moreover, for the yaw and roll velocities similar consideration can be carried out, showing their boundedness, but this is here omitted due to space limitation.

V. Simulations

The proposed control law has been derived starting from the simplified dynamic model (2). However, the birotor is continuously spinning around its vertical axis and some aerodynamic effects become not so negligible. In order to properly validate the controller, the more accurate dynamic model (1) has been hence considered to simulate the behaviour of the aerial vehicle.

In the following simulations, the employed dynamic parameters have been retrieved by experiments performed with off-the-shelf available quadrotors [22], [30]. In detail, the chosen mass and the inertia are 1.2 kg and $\text{diag}(3.4, 3.4, 4.7)\cdot 10^{-3}$ kgm^2, respectively. The parameters in (4) are $l = 0.21$ m, $\rho_u = 1.8 \cdot 10^{-5}$ Ns^2/rad^2 and $c = 8 \cdot 10^{-7}$ Nms^2/rad^2. The propeller's inertia is $I_p = 3.4 \cdot 10^{-5}$ kgm, and the term $\boldsymbol{g}_a$ in (1b) for the birotor is given by $I_p \boldsymbol{S}(\omega_b^b)\boldsymbol{e}_3(\omega_1 + \omega_3)$. A saturation for the maximum speed of the propellers w_i has been set to 630 rad/s (about 6000 rpm). The birotor at steady-state has a constant rotation speed of about 7 rad/s around its vertical axis. The friction coefficients in (1b) have been set to $\boldsymbol{F}_o = \text{diag}(0, 0, 7 \cdot 10^{-2})$ kgm^2/s.

The gains of the controller have been tuned by trial and error to $\boldsymbol{K}_p = \text{diag}(1.2, 1.2, 25)$, $\boldsymbol{K}_d = \text{diag}(1.6, 1.6, 8)$, $k_{p,\theta} = 25$ and $k_{d,\theta} = 50$. The integral actions have been put to $\text{diag}(0.5, 0.5, 10)$ for the linear components and 1 for the pitch control. The measurements and the control law are retrieved and given to the system, respectively, at each 10 ms.

Three case studies are considered in the following. Other case studies are included in the multimedia attachment. Without loss of generality, each planned trajectory ends in the origin of the Cartesian system Σ_i where the birotor stays for a while to evaluate steady-state performance. In the presented plots, the phase regarding the propellers turning-off is neglected.

1) Case Study A: In this case study, a straight line emergency landing trajectory is planned. Starting from $\boldsymbol{p}_b = \begin{bmatrix} 1 & 1 & 1 \end{bmatrix}^{\mathrm{T}}$m in Σ_i, the birotor has to reach the origin of the Cartesian system in 20 s. The initial and final velocities and accelerations are put to zero. A seventh-order polynomial has been employed for trajectory planning to guarantee the above defined conditions. The birotor stays for other 30 s in a steady-state condition.

Figs 3(a) and 3(b) show the time histories of the position error norm and the pitch error. The visible small oscillations are due to the continuous spinning of the birotor around its

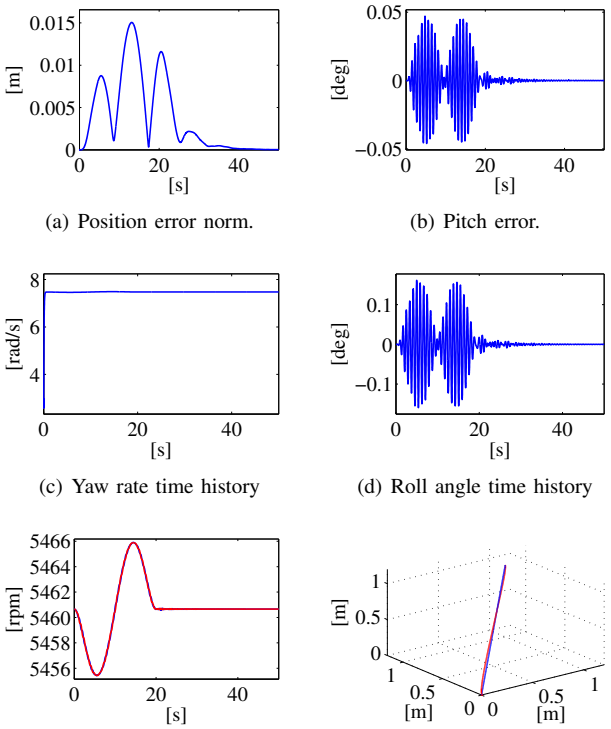

(a) Position error norm. (b) Pitch error.

(c) Yaw rate time history (d) Roll angle time history

(e) Commanded propeller velocities (f) 3D Cartesian path

Fig. 3. Case study A. Diagonal emergency landing trajectory. The norm error of the position and the pitch error are depicted in subfigures (a) and (b), respectively. The uncontrolled state variables are shown in subfigures (c), yaw angle velocity, and (d), roll angle. The commanded propeller velocities are represented in subfigure (e) with the following legend: blue, propeller 1; red, propeller 3. The 3D Cartesian planned path is shown in blue in subfigure (f), while the actual one is depicted in red.

vertical axis. The yaw angle velocity is depicted in Fig. 3(c), where the steady-state value is reached in less than 1 s (starting from a value of 3 rad/s). It might be possible to see a relationship between the oscillations in the error plots and the steady-state yaw velocity. Fixing the planned trajectory and the gains, varying the aerodynamic parameters c and ρ_u it is possible to modify (5) and hence the velocity in Fig. 3(c). Moreover, Fig. 3(d) shows that the uncontrolled roll angle remains limited. The commanded propeller velocities are depicted in Fig. 3(e) where it is possible to notice that their values do not saturate. The comparison between the planned 3D path and the actual one is represented in Fig. 3(f).

2) Case Study B: The same planned trajectory of case study A is employed but noise has been added to the measurements signals so as to simulate typical issues which could appear in the practice. In particular, a measurement white noise has been added to position (variance: $49 \cdot 10^{-6}$ m), linear velocity (variance: $25 \cdot 10^{-4}$ m/s), orientation (variance: $3 \cdot 10^{-4}$ rad) and angular velocity (variance: $2.7 \cdot 10^{-3}$ rad/s) measurements signals. Moreover, initial roll and pitch angles have been set to 4 degrees so as to simulate the case in which the tolerant control is switched-on and the initial conditions of both angles are reasonably nonzero.

The time histories are represented in Fig. 4. The stability is preserved showing some robustness properties of the developed control law. The uncontrolled variables remain

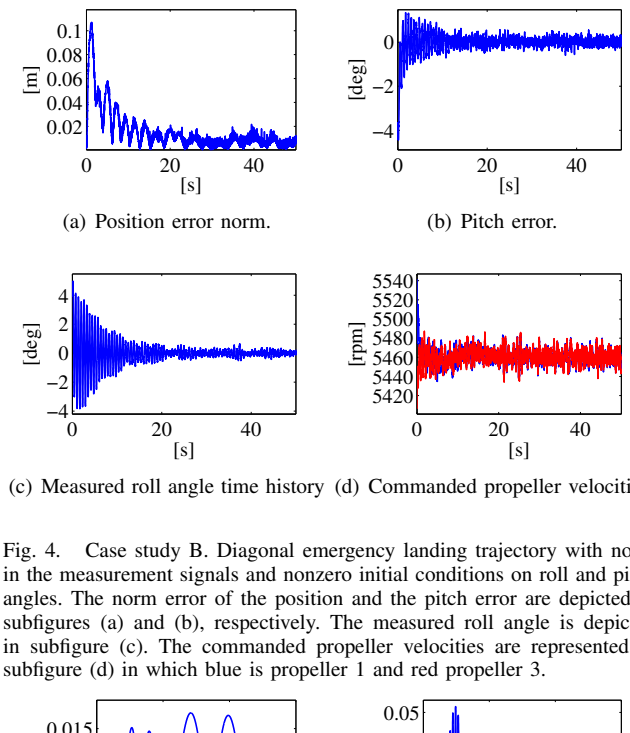

(a) Position error norm. (b) Pitch error.

(c) Measured roll angle time history (d) Commanded propeller velocities

Fig. 4. Case study B. Diagonal emergency landing trajectory with noise in the measurement signals and nonzero initial conditions on roll and pitch angles. The norm error of the position and the pitch error are depicted in subfigures (a) and (b), respectively. The measured roll angle is depicted in subfigure (c). The commanded propeller velocities are represented in subfigure (d) in which blue is propeller 1 and red propeller 3.

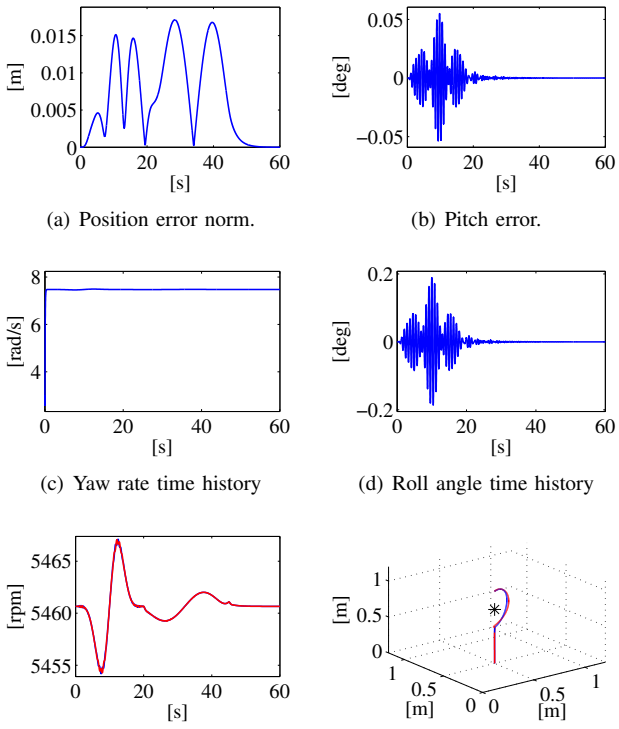

(a) Position error norm. (b) Pitch error.

(c) Yaw rate time history (d) Roll angle time history

(e) Commanded propeller velocities (f) 3D Cartesian path

Fig. 5. Case study C. Emergency landing trajectory with the presence of an obstacle. The norm error of the position and the pitch error are depicted in subfigures (a) and (b), respectively. The uncontrolled state variables are depicted in subfigures (c), yaw angle velocity, and (d), roll angle. The commanded propeller velocities are represented in subfigure (e) whose legend is: blue, propeller 1; red, propeller 3. The 3D Cartesian planned path is shown in blue in subfigure (f), the actual one is depicted in red, and the obstacle is represented with an asterisk.

bounded as well as the pitch and position errors.

3) Case Study C: In this case study, the presence of an obstacle along the emergency landing trajectory has been

simulated. The planned trajectory is first a semi-circle and then a vertical straight line towards the origin of the Cartesian system Σ_i, in such a way to avoid an obstacle. The circular path starts at the point $\boldsymbol{p}_1 = \begin{bmatrix}0.5 & 0.5 & 1\end{bmatrix}^{\mathrm{T}}$ m and it is planned to pass through $\boldsymbol{p}_2 = \begin{bmatrix}0.5 & 0.5 & 0.5\end{bmatrix}^{\mathrm{T}}$ m and $\boldsymbol{p}_3 = \begin{bmatrix}0.5 & 0.5 & 0\end{bmatrix}^{\mathrm{T}}$ m. Only half of this circle is followed. The duration of the trajectory upon this semi-circle is 20 s. Initial velocity and acceleration are set to zero, hence a seventh order polynomial for arclength parameterization has been employed. The vertical straight line lasts 25 s and the vehicle remains 15 s in steady-state.

Position error norm and the pitch error are shown in Figs 5(a) and 5(b), respectively. Yaw angle is depicted in Fig. 5(c), while roll time history is represented in-Fig. 5(d). The commanded propellers velocities are depicted in Fig. 5(e) where it is possible to notice again that their values do not saturate. The comparison between the planned 3D path and the actual one is represented in Fig. 5(f), where it is shown the planned semi-circle, the vertical straight line and the presence of the obstacle.

VI. Conclusion and future work

A controller dealing with problems related to the failure a quadrotor's propeller has been designed. The proposed solution considers to turn off also the motor on the same quadrotor axis of the broken propeller. With the proposed control law, the aerial vehicle can reach any point in the Cartesian space dropping the possibility to control the yaw angle. Any emergency landing trajectory can be then in principle considered. Future work will be focused on experimental evaluation and issues related to outdoor scenarios.

References

[1] [Online]. Available: http://www.amazon.com/b?node=8037720011

[2] V. Lippiello and B. Siciliano, "Wall inspection control of a VTOL unmanned aerial vehicle based on a stereo optical flow," in *2012 IEEE/RSJ International Conference on Intelligent Robots and Systems*, Vilamoura, P, 2012, pp. 4296–4302.

[3] P. Oh, M. Joyce, and J. Gallagher, "Designing an aerial robot for hover-and-stare surveillance," in *IEEE International Conference on Advanced Robotics*, Seattle, Wa, 2005, pp. 303–308.

[4] P. Pounds, D. Bersak, and A. Dollar, "Grasping from the air: Hovering capture and load stability," in *2011 IEEE International Conference on Robotics and Automation*, Shanghai, CN, 2011, pp. 2491–2498.

[5] G. Arleo, F. Caccavale, G. Muscio, and F. Pierri, "Control of quadrotor aerial vehicles equipped with a robotic arm," in *21st Mediterranean Conference on Control and Automation*, Crete, GR, 2013.

[6] V. Lippiello and F. Ruggiero, "Exploiting redundancy in Cartesian impedance control of UAVs equipped with a robotic arm," in *2012 IEEE/RSJ International Conference on Intelligent Robots and Systems*, Vilamoura, P, 2012, pp. 3768–3773.

[7] R. Mebarki, V. Lippiello, and B. Siciliano, "Exploiting image moments for aerial manipulation control," in *ASME Dynamic Systems and Control Conference*, Palo Alto, CA, 2013.

[8] V. Lippiello and F. Ruggiero, "Cartesian impedance control of a UAV with a robotic arm," in *10th International IFAC Symposium on Robot Control*, Dubrovnik, HR, 2012, pp. 704–709.

[9] M. Blanke, M. Staroswiecki, and N. Wu, "Concepts and methods in fault-tolerant control," in *2001 American Control Conference*, vol. 4, Arlington, VA, 2001, pp. 2606–2620.

[10] Y. Zhang and J. Jiang, "Bibliographical review on reconfigurable fault-tolerant control systems," *Annual Reviews in Control*, vol. 32, no. 2, pp. 229–252, 2008.

[11] C. Berbra, S. Lesecq, and J. Martinez, "A multi-observer switching strategy for fault-tolerant control of a quadrotor helicopter," in *16th Mediterranean Conference on Control and Automation*, Ajaccio, F, 2008, pp. 1094–1099.

[12] M. Mueller and R. D'Andrea, "Critical subsystem failure mitigation in an indoor UAV testbed," in *2012 IEEE/RSJ International Conference on Intelligent Robots and Systems*, Vilamoura, P, 2012, pp. 780–785.

[13] A. Freddi, S. Longhi, and A. Monteriu, "Actuator fault detection system for a mini-quadrotor," in *2010 IEEE International Symposium on Industrial Electronics*, Bari, I, 2010, pp. 2055–2060.

[14] M. Ranjbaran and K. Khorasani, "Fault recovery of an under-actuated quadrotor aerial vehicle," in *49th IEEE Conference on Decision and Control*, Atlanta, GA, 2010, pp. 4385–4392.

[15] F. Sharifi, M. Mirzaei, B. Gordon, and Y. Zhang, "Fault tolerant control of a quadrotor UAV using sliding mode control," in *2010 Conference on Control and Fault-Tolerant Systems*, Nice, F, 2010, pp. 239–244.

[16] I. Sadeghzadeh, A. Mehta, A. Chamseddine, and Y. Zhang, "Active fault tolerant control of a quadrotor UAV based on gain scheduled PID control," in *25th IEEE Canadian Conference on Electrical and Computer Engineering*, Montreal, QC, 2012, pp. 1–4.

[17] H. Khebbache, B. Sait, F. Yacef, and Y. Soukkou, "Robust stabilization of a quadrotor aerial vehicle in presence of actuator faults," *International Journal of Information Technology, Control and Automation*, vol. 2, no. 2, pp. 1–13, 2012.

[18] Y. Zhang and A. Chamseddine, "Fault tolerant flight control techniques with application to a quadrotor UAV testbed," in *Automatic Flight Control Systems - Latest Developments*, T. Lombaerts, Ed. InTech, 2012, pp. 119–150.

[19] A. Freddi, A. Lanzon, and S. Longhi, "A feedback linearization approach to fault tolerance in quadrotor vehicles," in *18th IFAC World Congress*, Milano, I, 2011, pp. 5413–5418.

[20] Y. Kataoka, K. Sekiguchi, and M. Sampei, "Nonlinear control and model analysis of trirotor UAV model," in *18th IFAC World Congress*, Milano, I, 2011, pp. 10 391–10 396.

[21] A. Lanzon, A. Freddi, and S. Longhi, "Flight control of a quadrotor vehicle subsequent to a rotor failure," *Journal of Guidance, Control, and Dynamics*, vol. 37, no. 2, pp. 580–591, 2014.

[22] M. Mueller and R. D'Andrea, "Stability and control of a quadrocopter despite the complete loss of one, two, or three propellers," in *2014 IEEE International Conference on Robotics and Automation*, Hong Kong, C, 2014, pp. 45–52.

[23] N. Amiri, A. Ramirez-Serrano, and R. Davies, "Modelling of opposed lateral and longitudinal tilting dual-fan unmanned aerial vehicle," in *18th IFAC World Congress*, Milano, I, 2011, pp. 2054–2059.

[24] C. Papachristos, K. Alexis, and A. Tzes, "Design and experimental attitude control of an unmanned tilt-rotor aerial vehicle," in *15th International Conference on Advanced Robotics*, Tallin, EST, 2011, pp. 465–470.

[25] V. Lippiello, F. Ruggiero, and D. Serra, "Emergency landing for a quadrotor in case of propeller fault: A backstepping approach," in *2014 IEEE/RSJ International Conference on Intelligent Robots and Systems (accepted for publication)*, Chicago, IL, 2014.

[26] B. Siciliano, L. Sciavicco, L. Villani, and G. Oriolo, *Robotics: Modelling, Planning and Control*. London, UK: Springer, 2008.

[27] T. Hamel, R. Mahony, R. Lozano, and J. Ostrowski, "Dynamic modelling and configuration stabilization for an X4-flyer," in *15th IFAC World Congress*, Barcelona, E, 2002, pp. 846–851.

[28] K. Nonami, F. Kendoul, S. Suzuki, and W. Wang, *Autonomous Flying Robots. Unmanned Aerial Vehicles and Micro Aerial Vehicles*. Berlin Heidelberg, D: Springer-Verlag, 2010.

[29] H. Khalil, *Nonlinear systems*. Upper Saddle River, NJ: Prentice Hall, 2002.

[30] F. Ruggiero, J. Cacace, H. Sadeghian, and V. Lippiello, "Impedance control of VTOL UAVs with a momentum-based external generalized forces estimator," in *2014 IEEE International Conference on Robotics and Automation*, Hong Kong, C, 2014, pp. 2093–2099.